JOURNAL OF MOLECULAR SPECTROSCOPY 56, 210–228 (1975)

Analysis of the Laser Magnetic Resonance Spectrum of HO_2

J. T. HOUGEN

National Bureau of Standards, Washington, D. C. 20234

H. E. RADFORD

Harvard College Observatory and Smithsonian Astrophysical Observatory, Cambridge, Massachusetts 02138

K. M. EVENSON

National Bureau of Standards, Boulder, Colorado 80302

AND

CARLETON J. HOWARD

Aeronomy Laboratory, NOAA Environmental Research Laboratories, Boulder, Colorado 80302

An analysis of the previously detected laser magnetic resonance spectrum of HO_2 is carried out by (i) assigning M_J quantum numbers to each observed Zeeman line, (ii) determining the quantum numbers $(N'_{K_a'K_c'}-N''_{K_a''K_c''})$ and energies of the zero-field asymmetric rotor transitions involved, and (iii) determining the values of the zero-field spin–rotation doublet splittings in the upper and lower states of each asymmetric rotor transition. The rotational transitions obtained lie in the region 50–150 cm^{-1}, with quantum numbers $4 \leq N \leq 19$ and $1 \leq K_a \leq 4$. They are fit to an asymmetric rotor program to obtain the three rotational constants A, B, C and the three symmetric-top centrifugal distortion constants D_K, D_{NK}, D_N. The spin splittings are fit to an approximate theoretical expression involving two adjustable linear combinations of components of the spin–rotation interaction tensor $\boldsymbol{\varepsilon}$. Because of the lack of spectra from other isotopic species, a unique molecular geometry cannot be derived.

I. INTRODUCTION

The laser magnetic resonance spectrum of HO_2 has recently been detected (*1*). Rather extensive spectra were obtained, prompting the development of a theoretical formalism for aiding in making initial assignments (*2*). The present paper gives a spectroscopic analysis of the data existing at present, though all observed Zeeman transitions are by no means assigned, and deviations between observed and calculated Zeeman fields are still significantly larger than experimental error and quite systematic. The present analysis leads to a set of zero-field asymmetric rotor energy levels for HO_2 and to a set of zero-field spin–rotational doublet splittings.

The initial analysis of a magnetic resonance spectrum obtained with a given laser line can be somewhat complicated, and the reader is referred to Ref. (*2*) for more details. Briefly, however, such analysis involves (i) separate consideration of the π spectrum and the σ spectrum, where the π and σ spectra have the electric field vector of the laser

radiation parallel to and perpendicular to the external magnetic field direction, respectively; (ii) grouping of Zeeman lines within the π or σ spectrum into plausible branches; (iii) fitting the π branches to

$$H^2 = aM_J{}^2H^2 + b_{\text{eff}}M_JH + c \tag{1}$$

for various trial M_J numberings of the branches, and fitting the σ branches to

$$H^2 = (a^{\frac{1}{2}}M_J + d_{\text{eff}})^2H^2 + (b_{\text{eff}}M_J - e_{\text{eff}})H + c \tag{2}$$

for a single M_J numbering, using the values of a, b_{eff}, and c determined from the π branch fits; (iv) determination of values for a, b, c, d, e from the effective constants obtained in the fitting procedure, with subsequent determination of values for the zero-field molecular transition frequency ($\nu_{\text{laser}} - \Delta E$), the upper- and lower-state spin splittings ($2\delta'$ and $2\delta''$), and the upper- and lower-state rotational quantum numbers (N' and N''), using Eqs. (3) with $g = 2.00232$ and $\mu_B = 0.046\,686$ cm^{-1}/kG,

$$\begin{aligned}
a &= [\delta'/(N' + \tfrac{1}{2}) - \delta''/(N'' + \tfrac{1}{2})]^2/\Delta E^2,\\
(g\mu_B)b &= 2[\delta'/(N' + \tfrac{1}{2}) - \delta''/(N'' + \tfrac{1}{2})](\delta'^2 - \delta''^2)/\Delta E^2\\
&\qquad - 2[\delta'/(N' + \tfrac{1}{2}) + \delta''/(N'' + \tfrac{1}{2})],\\
(g\mu_B)^2c &= \Delta E^2 - 2(\delta'^2 + \delta''^2) + (\delta'^2 - \delta''^2)^2/\Delta E^2,\\
d &= \delta'/(N' + \tfrac{1}{2})\Delta E,\\
(g\mu_B)e &= 2[\delta'/(N' + \tfrac{1}{2})\Delta E^2][\Delta E^2 - (\delta'^2 - \delta''^2)];
\end{aligned} \tag{3}$$

(v) a final least-squares fitting of the assigned spectrum to

$$\begin{aligned}
0 = \Delta E &- (\pm)[\delta'^2 + \delta' M_J' g\mu_B H/(N' + \tfrac{1}{2}) + \tfrac{1}{4}g^2\mu_B{}^2H^2]^{\frac{1}{2}}\\
&+ (\pm)[\delta''^2 + \delta'' M_J'' g\mu_B H/(N'' + \tfrac{1}{2}) + \tfrac{1}{4}g^2\mu_B{}^2H^2]^{\frac{1}{2}}.
\end{aligned} \tag{4}$$

Figure 1 illustrates the quantities ν_{laser}, ΔE, δ', and δ''.

Figures 3–5 of Ref. (*2*) illustrate three mutually exclusive cases according to which the Zeeman spectra in this paper can conveniently be classified. These cases correspond respectively to

$$|\Delta E| < |(|\delta'| - |\delta''|)|, \tag{5a}$$

$$|(|\delta'| - |\delta''|)| < |\Delta E| < |\delta'| + |\delta''|, \tag{5b}$$

$$|\delta'| + |\delta''| \quad < |\Delta E|, \tag{5c}$$

i.e., correspond to situations in which the mismatch $|\Delta E|$ between the laser frequency and the molecular transition is smaller than the difference in upper- and lower-state spin-splitting parameters, is larger than the difference but smaller than the sum or is larger than the sum.

After each Zeeman pattern has been assigned and subjected to a least-squares computer fit using the formalism described above and in Ref. (*2*), the resulting set of asymmetric rotor transitions and the set of spin–rotational doublet splittings are also subjected to least-squares computer fits using standard theoretical models as described in Sections IV and V.

During the course of fitting an *individual* Zeeman pattern, two kinds of uncertainties in assignment can arise, as mentioned in Section III. The less serious problem involves

uncertainties of one or two units in the N, K_a, or K_c numbering. For these cases, an unambiguous choice among the several possible values for the quantum numbers can normally be achieved by requiring the resultant zero-field asymmetric rotor transition frequency and assignment to be consistent with zero-field data from more securely assigned Zeeman patterns. The more serious problem involves uncertainties of one or two units in the M_J numbering of the Zeeman branches. For these cases, no technique for choosing among the several possible M_J numberings was discovered, and data from Zeeman patterns exhibiting such uncertainties were not used in the final asymmetric rotor and spin-splitting fits.

II. EXPERIMENTAL DETAILS

Laser magnetic resonance spectra were recorded using modifications of the original instrument (*3*) as described in Ref. (*1*) and references therein. For carefully measured lines the magnetic field was tuned to the line center and measured directly with an NMR proton gaussmeter *in situ*. A small correction for the NMR probe location was made. For these carefully measured lines the laser frequency was retuned before each measurement to maximize the output power, giving an approximate frequency reproducibility of 1 MHz. Magnetic fields of the carefully measured lines are given to 0.1 G in Table 1. Because of the combined uncertainties of magnetic field measurement and laser frequency variation, they are probably reliable to ± 0.5 G. Magnetic fields of many other lines were determined from chart measurements with a ruler. Since the dispersion of the measured charts was about 7 G/mm, these fields are given in Table 1 to 1 G; they are probably reliable to ± 5 G. Magnetic field values above 17 kG, where the NMR proton gaussmeter could no longer be used, were determined very unreliably and are not given in this paper.

Absolute frequencies of seven H_2O and D_2O laser lines have recently been remeasured (*4*). Frequencies, wavelengths, and wavenumbers for these lines are reproduced here in Table 2.

III. DISCUSSION OF INDIVIDUAL ZEEMAN PATTERNS

Individual Zeeman patterns are grouped in this paper according to the fixed-frequency laser line used as a radiation source. The laser lines are discussed below in order of increasing complexity of their associated spectral analysis; they are arranged in the Zeeman line list, Tables 1-A to 1-U, in order of increasing frequency.

The notation (*2*) used in Table 1 is as follows. Each subtable has a heading specifying the asymmetric rotor transition (*5*) $N'(K_a', K_c')$–$N''(K_a'', K_c'')$, the laser wavenumber in cm^{-1}, and the relationship between the external magnetic field direction and the electric field vector of the laser radiation (parallel or perpendicular). The measured field values H are given in kilogauss. The values $\Delta H \equiv H_{obs} - H_{calc}$ as obtained for each line from the least-squares fit using Eq. (4) are given in Gauss. The assignment PAB(−8.5) in Table 1-D, for example, represents a transition with $\Delta M_J = -1$(P), between the higher energy component (A) of the upper-state spin doublet and the lower-energy component (B) of the lower-state spin doublet, arising from a lower-state rotational level with $M_J = -8.5$. Note that the computer-printed PAB(−8.5) in Table 1 corresponds in the text to $P_{ab}(-8.5)$.

TABLE 1 THE LASER MAGNETIC RESONANCE SPECTRUM OF HO_2 - SEE END OF TABLE FOR NOTATION

TABLE 1-A
8(2,7)-8(1,8)
LASER = 58.625 CM-1
PARALLEL SPECTRUM

H (KG)	ΔH(G)	ASSIGNMENT
6.4930	0	QBB(3.5)
5.9830	-1	QBB(4.5)
5.5910	-3	QBB(5.5)
5.2980	-4	QBB(6.5)
5.0950	-8	QBB(7.5)

PERPENDICULAR SPECTRUM

H (KG)	ΔH(G)	ASSIGNMENT
12.1570	5	RBB(-2.5)
9.8610	1	RBB(-1.5)
8.3690	2	RBB(-0.5)
7.3210	0	RBB(0.5)
6.5530	1	RBB(1.5)
5.9650	-1	RBB(2.5)
5.5070	-6	RBB(3.5)
5.1540	-5	RBB(4.5)
4.8770	-9	RBB(5.5)
4.6690	-15	RBB(6.5)
12.5870	-20	PBB(0.5)
10.3830	9	PBB(1.5)
8.9050	11	PBB(2.5)
7.8600	10	PBB(3.5)
7.0960	12	PBB(4.5)
6.5190	9	PBB(5.5)
6.0870	6	PBB(6.5)
5.7790	6	PBB(7.5)

TABLE 1-B
4(3,2)-5(2,3)
LASER = 84.323 CM-1
PARALLEL SPECTRUM

H (KG)	ΔH(G)	ASSIGNMENT
18.0002	-37	QBB(-0.5)
14.3062	-32	QBB(0.5)
12.1621	-24	QBB(1.5)
10.8278	-21	QBB(2.5)
10.0300	-16	QBB(3.5)
9.7257	-13	QBB(4.5)

PERPENDICULAR SPECTRUM

H (KG)	ΔH(G)	ASSIGNMENT
17.905	13	PBB(2.5)
16.0995	16	PBB(3.5)
15.6519	34	PBB(4.5)
15.493	60	RBB(-2.5)
11.8710	12	RBB(-1.5)
9.8333	1	RBB(-0.5)
8.528	-2	RBB(0.5)
7.6303	-4	RBB(1.5)

TABLE 1-C
4(3,1)-5(2,4)
LASER = 84.323 CM-1
PARALLEL SPECTRUM

H (KG)	ΔH(G)	ASSIGNMENT
17.6217	-34	QBB(-0.5)
14.0255	-30	QBB(0.5)
11.9329	-23	QBB(1.5)
10.6322	-17	QBB(2.5)
9.8484	-16	QBB(3.5)
9.5471	-14	QBB(4.5)

PERPENDICULAR SPECTRUM

H (KG)	ΔH(G)	ASSIGNMENT
17.6653	11	PBB(2.5)
15.9080	15	PBB(3.5)
15.4944	32	PBB(4.5)
15.0529	55	RBB(-2.5)
11.5659	14	RBB(-1.5)
9.5935	3	RBB(-0.5)
8.3225	-4	RBB(0.5)
7.452	-3	RBB(1.5)

TABLE 1-D
13(2,12)-12(1,11)
LASER = 84.323 CM-1
PARALLEL SPECTRUM

H (KG)	ΔH(G)	ASSIGNMENT
2.749	-5	QAB(-12.5)
2.895	-4	QAB(-11.5)
3.053	-4	QAB(-10.5)
3.226	-2	QAB(-9.5)
3.415	0	QAB(-8.5)
3.616	-3	QAB(-7.5)
3.840	-1	QAB(-6.5)
4.083	0	QAB(-5.5)
4.348	1	QAB(-4.5)
4.633	0	QAB(-3.5)
4.942	-1	QAB(-2.5)
5.276	-4	QAB(-1.5)
5.642	-3	QAB(-0.5)
6.039	0	QAB(0.5)
6.464	2	QAB(1.5)
6.921	5	QAB(2.5)
7.405	4	QAB(3.5)
7.919	0	QAB(4.5)
8.475	3	QAB(5.5)
9.063	5	QAB(6.5)
9.689	9	QAB(7.5)
10.350	10	QAB(8.5)
11.049	11	QAB(9.5)
11.792	16	QAB(10.5)
12.573	16	QAB(11.5)

PERPENDICULAR SPECTRUM

H (KG)	ΔH(G)	ASSIGNMENT
3.312	5	PAB(-8.5)
3.509	9	PAB(-7.5)
3.718	7	PAB(-6.5)
3.948	8	PAB(-5.5)
4.192	2	PAB(-4.5)
4.471	10	PAB(-3.5)
4.763	7	PAB(-2.5)
5.086	10	PAB(-1.5)
5.431	9	PAB(-0.5)
5.804	10	PAB(0.5)
6.191	-4	PAB(1.5)
3.337	1	RAB(-9.5)
3.534	1	RAB(-8.5)
3.749	1	RAB(-7.5)
3.983	1	RAB(-6.5)
4.239	2	RAB(-5.5)
4.515	0	RAB(-4.5)
4.817	0	RAB(-3.5)
5.144	-1	RAB(-2.5)
5.498	-3	RAB(-1.5)
5.881	-5	RAB(-0.5)
6.296	-5	RAB(0.5)
6.744	-4	RAB(1.5)
7.220	-7	RAB(2.5)
7.731	-9	RAB(3.5)
8.277	-11	RAB(4.5)
8.859	-12	RAB(5.5)
9.483	-9	RAB(6.5)
10.146	-5	RAB(7.5)
10.840	-10	RAB(8.5)
11.579	-13	RAB(9.5)
12.367	-11	RAB(10.5)
13.216	3	RAB(11.5)

TABLE 1-E
11(2,9)-10(1,10)
LASER ◘ 84.323 CM-1
PARALLEL SPECTRUM

H (KG)	ΔH(G)	ASSIGNMENT
4.109	0	QAB(-10.5)
4.322	1	QAB(-9.5)
4.550	0	QAB(-8.5)
4.797	0	QAB(-7.5)
5.060	-4	QAB(-6.5)
5.347	-7	QAB(-5.5)
5.664	-4	QAB(-4.5)
6.006	-1	QAB(-3.5)
6.375	0	QAB(-2.5)
6.779	7	QAB(-1.5)
7.203	2	QAB(-0.5)
7.661	-2	QAB(0.5)
8.162	-1	QAB(1.5)
8.707	3	QAB(2.5)
9.293	6	QAB(3.5)
9.920	5	QAB(4.5)
10.600	7	QAB(5.5)
11.335	9	QAB(6.5)
12.132	15	QAB(7.5)
12.996	22	QAB(8.5)
13.932	29	QAB(9.5)

PERPENDICULAR SPECTRUM

H (KG)	ΔH(G)	ASSIGNMENT
4.412	11	PAB(-8.5)
4.643	7	PAB(-7.5)
4.896	7	PAB(-6.5)
5.173	10	PAB(-5.5)
5.471	12	PAB(-4.5)
5.789	9	PAB(-3.5)
6.137	11	PAB(-2.5)
6.511	12	PAB(-1.5)
6.919	16	PAB(-0.5)
7.353	15	PAB(0.5)
7.819	11	PAB(1.5)
4.706	-2	RAB(-8.5)
4.969	0	RAB(-7.5)
5.251	-2	RAB(-6.5)
5.556	-4	RAB(-5.5)
5.888	-5	RAB(-4.5)
6.249	-4	RAB(-3.5)
6.639	-4	RAB(-2.5)
7.061	-5	RAB(-1.5)
7.512	-11	RAB(-0.5)
8.005	-13	RAB(0.5)
8.539	-13	RAB(1.5)
9.114	-17	RAB(2.5)
9.736	-20	RAB(3.5)
10.416	-16	RAB(4.5)
11.146	-17	RAB(5.5)
11.933	-22	RAB(6.5)
12.803	-12	RAB(7.5)
13.742	-7	RAB(8.5)
14.766	0	RAB(9.5)

TABLE 1-F
14(2,13)-13(1,12)
LASER ◘ 84.323 CM-1
PARALLEL SPECTRUM

H (KG)	ΔH(G)	ASSIGNMENT
6.335	-2	QBA(-7.5)
6.592	-1	QBA(-6.5)
6.866	3	QBA(-5.5)
7.150	3	QBA(-4.5)
7.442	-3	QBA(-3.5)
7.755	-4	QBA(-2.5)
8.086	-4	QBA(-1.5)
8.437	-1	QBA(-0.5)
8.803	0	QBA(0.5)
9.190	2	QBA(1.5)
9.593	3	QBA(2.5)
10.011	0	QBA(3.5)
10.455	2	QBA(4.5)
10.917	2	QBA(5.5)
11.401	3	QBA(6.5)
11.910	7	QBA(7.5)
12.433	2	QBA(8.5)
12.996	14	QBA(9.5)
13.574	16	QBA(10.5)
14.179	21	QBA(11.5)
14.811	26	QBA(12.5)

PERPENDICULAR SPECTRUM

H (KG)	ΔH(G)	ASSIGNMENT
6.437	6	PBA(-6.5)
6.704	13	PBA(-5.5)
6.976	12	PBA(-4.5)
7.258	6	PBA(-3.5)
7.561	6	PBA(-2.5)
7.880	6	PBA(-1.5)
8.216	8	PBA(-0.5)
8.569	9	PBA(0.5)
8.941	12	PBA(1.5)
9.333	17	PBA(2.5)
8.669	-12	RBA(-0.5)
9.049	-12	RBA(0.5)
9.451	-9	RBA(1.5)
9.865	-13	RBA(2.5)
10.307	-10	RBA(3.5)
10.762	-15	RBA(4.5)
11.238	-20	RBA(5.5)
11.744	-18	RBA(6.5)
12.267	-22	RBA(7.5)
12.829	-11	RBA(8.5)
13.407	-9	RBA(9.5)
14.010	-7	RBA(10.5)
14.641	-5	RBA(11.5)

TABLE 1-G
12(2,10)-11(1,11)
LASER = 84.323 CM-1
PARALLEL SPECTRUM

H (KG)	ΔH(G)	ASSIGNMENT
13.791	4	QBA(-5.5)
14.147	-2	QBA(-4.5)
14.519	-5	QBA(-3.5)
14.902	-10	QBA(-2.5)
15.307	-7	QBA(-1.5)
15.725	-6	QBA(-0.5)
16.160	-2	QBA(0.5)
16.618	0	QBA(1.5)
17.091	20	QBA(2.5)
17.580	31	QBA(3.5)

PERPENDICULAR SPECTRUM

H (KG)	ΔH(G)	ASSIGNMENT
12.562	17	PBA(-8.5)
12.880	17	PBA(-7.5)
13.202	11	PBA(-6.5)
13.538	7	PBA(-5.5)
13.882	0	PBA(-4.5)
14.245	-2	PBA(-3.5)
14.623	0	PBA(-2.5)
15.007	-7	PBA(-1.5)
15.412	-5	PBA(-0.5)
15.830	-5	PBA(0.5)
16.268	0	PBA(1.5)
16.722	6	PBA(2.5)
15.204	-8	RBA(-2.5)
15.611	-16	RBA(-1.5)
16.042	-15	RBA(-0.5)
16.489	-13	RBA(0.5)
16.958	-4	RBA(1.5)
17.446	5	RBA(2.5)

TABLE 1-H
18(4,15)-19(3,16)
LASER = 92.833 CM-1
PARALLEL SPECTRUM

H (KG)	ΔH(G)	ASSIGNMENT
17.1300	-6	QAA(11.5)
16.425	-3	QAA(12.5)
15.811	1	QAA(13.5)
15.275	3	QAA(14.5)
14.8157	4	QAA(15.5)
14.4377	5	QAA(16.5)
14.144	-2	QAA(17.5)

PERPENDICULAR SPECTRUM

H (KG)	ΔH(G)	ASSIGNMENT
17.3327	2	PAA(14.5)
16.723	4	PAA(15.5)
16.211	3	PAA(16.5)
15.808	1	PAA(17.5)
15.5387	-8	PAA(18.5)

TABLE 1-I
18(4,14)-19(3,17)
LASER = 92.833 CM-1
PARALLEL SPECTRUM

H (KG)	ΔH(G)	ASSIGNMENT
17.8335	-7	QAA(11.5)
17.047	-1	QAA(12.5)
16.356	1	QAA(13.5)
15.751	2	QAA(14.5)
15.2304	5	QAA(15.5)
14.791	5	QAA(16.5)
14.4377	-1	QAA(17.5)

PERPENDICULAR SPECTRUM

H (KG)	ΔH(G)	ASSIGNMENT
17.9158	7	PAA(14.5)
17.216	1	PAA(15.5)
16.6271	0	PAA(16.5)
16.152	0	PAA(17.5)
15.808	-6	PAA(18.5)

TABLE 1-J
15(2,13)-14(1,14)
LASER = 92.833 CM-1
PARALLEL SPECTRUM

H (KG)	ΔH(G)	ASSIGNMENT
6.146	3	QBA(-11.5)
6.331	7	QBA(-10.5)
6.520	6	QBA(-9.5)
6.719	8	QBA(-8.5)
6.925	8	QBA(-7.5)
7.141	9	QBA(-6.5)
7.364	7	QBA(-5.5)
7.587	-3	QBA(-4.5)
7.828	-6	QBA(-3.5)
8.083	-6	QBA(-2.5)
8.351	-4	QBA(-1.5)
8.627	-5	QBA(-0.5)
8.916	-6	QBA(0.5)
9.223	-2	QBA(1.5)
9.539	-2	QBA(2.5)
9.866	-4	QBA(3.5)
10.208	-7	QBA(4.5)
10.570	-5	QBA(5.5)
10.952	0	QBA(6.5)
11.3466	1	QBA(7.5)
11.765	8	QBA(8.5)
12.199	11	QBA(9.5)
12.6473	9	QBA(10.5)
13.121	11	QBA(11.5)
13.616	11	QBA(12.5)
14.133	9	QBA(13.5)

PERPENDICULAR SPECTRUM

H (KG)	ΔH(G)	ASSIGNMENT
5.857	5	PBA(-12.5)
6.025	4	PBA(-11.5)
6.202	6	PBA(-10.5)
6.385	5	PBA(-9.5)
6.578	7	PBA(-8.5)
6.778	8	PBA(-7.5)
6.988	10	PBA(-6.5)
7.200	5	PBA(-5.5)
7.4227	2	PBA(-4.5)
7.6590	3	PBA(-3.5)
7.903	1	PBA(-2.5)
8.160	1	PBA(-1.5)
8.430	4	PBA(-0.5)
8.7096	4	PBA(0.5)
9.002	6	PBA(1.5)
9.309	9	PBA(2.5)
9.626	9	PBA(3.5)
9.954	6	PBA(4.5)
10.303	9	PBA(5.5)
10.668	13	PBA(6.5)
11.048	16	PBA(7.5)
11.445	20	PBA(8.5)
11.862	25	PBA(9.5)
7.999	-22	RBA(-3.5)
8.272	-13	RBA(-2.5)
8.551	-10	RBA(-1.5)
8.840	-10	RBA(-0.5)
9.138	-13	RBA(0.5)
9.453	-13	RBA(1.5)
9.780	-15	RBA(2.5)
10.1223	-16	RBA(3.5)
10.481	-16	RBA(4.5)
10.857	-16	RBA(5.5)
11.253	-13	RBA(6.5)
11.666	-11	RBA(7.5)
12.099	-8	RBA(8.5)
12.5473	-11	RBA(9.5)
13.0223	-8	RBA(10.5)
13.522	-4	RBA(11.5)
14.044	-2	RBA(12.5)
14.594	0	RBA(13.5)

CONTINUED

TABLE 1 CONTINUED

TABLE 1-K
11(3,8)-10(2,9)
LASER = 118.654 CM-1
PARALLEL SPECTRUM

H (KG)	ΔH(G)	ASSIGNMENT
8.0110	-8	QBA(4.5)
11.1900	-6	QBA(5.5)
14.1013	1	QBA(6.5)
16.9780	19	QBA(7.5)
2.5548	-10	QBA(4.5)
1.858	4	QBA(5.5)
1.489	1	QBA(6.5)

PERPENDICULAR SPECTRUM

H (KG)	ΔH(G)	ASSIGNMENT
5.8278	7	RBA(3.5)
9.7185	-18	RBA(4.5)
12.7957	-23	RBA(5.5)
15.7743	-19	RBA(6.5)
9.6649	-5	PBA(5.5)
12.5875	11	PBA(6.5)
15.3850	33	PBA(7.5)

TABLE 1-L
11(3,9)-10(2,8)
LASER = 118.654 CM-1
PARALLEL SPECTRUM

H (KG)	ΔH(G)	ASSIGNMENT
8.0732	-11	QBA(5.5)
12.2116	1	QBA(6.5)
15.5020	19	QBA(7.5)
4.8365	-2	QBA(5.5)
3.2380	-3	QBA(6.5)
2.589	-2	QBA(7.5)

PERPENDICULAR SPECTRUM

H (KG)	ΔH(G)	ASSIGNMENT
10.4508	-17	RBA(5.5)
14.0832	-15	RBA(6.5)
17.4213	-4	RBA(7.5)
3.8321	-9	RBA(5.5)
2.8906	-7	RBA(6.5)
2.383	-5	RBA(7.5)
2.050	0	RBA(8.5)
10.403	1	PBA(6.5)
13.791	29	PBA(7.5)

TABLE 1-M
10(3,7)-9(2,8)
LASER = 118.654 CM-1
PARALLEL SPECTRUM

H (KG)	ΔH(G)	ASSIGNMENT
13.3591	1	QAB(8.5)
6.8100	-8	QAB(9.5)

PERPENDICULAR SPECTRUM

H (KG)	ΔH(G)	ASSIGNMENT
8.2136	7	RAB(8.5)
18.273	0	RAB(8.5)

TABLE 1-N
10(3,8)-9(2,7)
LASER = 118.654 CM-1
PARALLEL SPECTRUM

H (KG)	ΔH(G)	ASSIGNMENT
15.4148	1	QAB(8.5)
6.2467	-5	QAB(9.5)

PERPENDICULAR SPECTRUM

H (KG)	ΔH(G)	ASSIGNMENT
7.3080	5	RAB(8.5)
19.481	0	RAB(8.5)

TABLE 1-O
14(3,12)-13(2,11)
LASER = 126.437 CM-1
PARALLEL SPECTRUM

H (KG)	ΔH(G)	ASSIGNMENT
17.5359	-80	QAA(-1.5)
16.0686	-36	QAA(-0.5)
14.8871	-11	QAA(0.5)
13.9224	2	QAA(1.5)
13.1249	10	QAA(2.5)
12.4595	14	QAA(3.5)
11.9028	14	QAA(4.5)
11.4379	13	QAA(5.5)
11.0527	10	QAA(6.5)
10.7392	6	QAA(7.5)
10.4942	1	QAA(8.5)
10.3180	-5	QAA(9.5)
10.2144	-17	QAA(10.5)
10.2144	-21	QAA(11.5)
10.337	-44	QAA(12.5)

PERPENDICULAR SPECTRUM

H (KG)	ΔH(G)	ASSIGNMENT
16.534	-13	PAA(2.5)
15.4425	4	PAA(3.5)
14.5537	18	PAA(4.5)
13.8205	26	PAA(5.5)
13.2148	27	PAA(6.5)
12.7191	26	PAA(7.5)
12.3207	22	PAA(8.5)
12.0139	16	PAA(9.5)
14.4819	8	RAA(-2.5)
13.439	14	RAA(-1.5)
12.591	27	RAA(-0.5)
11.8739	24	RAA(0.5)
11.2740	23	RAA(1.5)
10.7665	22	RAA(2.5)
10.3356	19	RAA(3.5)
9.9692	14	RAA(4.5)
9.6625	10	RAA(5.5)
9.4087	5	RAA(6.5)
9.2050	0	RAA(7.5)
9.0528	-5	RAA(8.5)
8.9545	-12	RAA(9.5)
8.9200	-22	RAA(10.5)
8.9745	-35	RAA(11.5)
9.1761	-54	RAA(12.5)

TABLE 1-P
14(3,11)-13(2,12)
LASER = 126.437 CM-1
PARALLEL SPECTRUM

H (KG)	ΔH(G)	ASSIGNMENT
17.3463	-34	QAA(10.5)
15.9607	-4	QAA(11.5)
14.7891	14	QAA(12.5)
13.7906	26	QAA(13.5)
16.8586	-18	QBB(11.5)
15.4407	9	QBB(12.5)

PERPENDICULAR SPECTRUM

H (KG)	ΔH(G)	ASSIGNMENT
16.8528	-29	RAA(8.5)
15.5285	-4	RAA(9.5)
14.4026	12	RAA(10.5)
13.4373	26	RAA(11.5)
12.5981	30	RAA(12.5)
16.5160	-30	RBB(9.5)
15.1667	-3	RBB(10.5)
14.0115	15	RBB(11.5)
13.0064	26	RBB(12.5)

TABLE 1-Q
14(3,12)-13(2,11)
LASER = 127.481 CM-1
PARALLEL SPECTRUM

H (KG)	ΔH(G)	ASSIGNMENT
1.557	5	QAB(-13.5)
1.667	8	QAB(-12.5)
1.790	11	QAB(-11.5)
1.925	8	QAB(-10.5)
2.081	6	QAB(-9.5)
2.261	3	QAB(-8.5)
2.470	0	QAB(-7.5)
2.715	-4	QAB(-6.5)
3.008	-4	QAB(-5.5)
3.361	1	QAB(-4.5)
3.772	0	QAB(-3.5)
4.261	3	QAB(-2.5)
4.832	2	QAB(-1.5)
5.492	-5	QAB(-0.5)
6.265	0	QAB(0.5)
7.142	3	QAB(1.5)
8.112	0	QAB(2.5)
9.184	3	QAB(3.5)
10.3451	6	QAB(4.5)
11.590	11	QAB(5.5)
12.904	9	QAB(6.5)
14.301	20	QAB(7.5)
15.753	17	QAB(8.5)
17.286	28	QAB(9.5)

PERPENDICULAR SPECTRUM

H (KG)	ΔH(G)	ASSIGNMENT
2.864	0	RAB(-6.5)
3.185	1	RAB(-5.5)
3.569	6	RAB(-4.5)
4.013	0	RAB(-3.5)
4.548	4	RAB(-2.5)
5.1658	0	RAB(-1.5)
5.889	-1	RAB(-0.5)
6.717	-1	RAB(0.5)
7.646	-6	RAB(1.5)
8.679	-9	RAB(2.5)
9.8086	-11	RAB(3.5)
11.029	-12	RAB(4.5)
12.3303	-15	RAB(5.5)
13.714	-14	RAB(6.5)
15.1676	-17	RAB(7.5)
16.695	-19	RAB(8.5)

TABLE 1-R
14(3,11)-13(2,12)
LASER = 127.481 CM-1
PARALLEL SPECTRUM

H (KG)	ΔH(G)	ASSIGNMENT
1.074	0	QAB(8.5)
0.944	2	QAB(9.5)
0.841	0	QAB(10.5)
0.758	-1	QAB(11.5)
0.695	1	QAB(12.5)
0.640	1	QAB(13.5)
8.351	9	QAB(6.5)
10.231	8	QAB(7.5)
12.073	16	QAB(8.5)
13.906	16	QAB(9.5)
15.771	21	QAB(10.5)
17.680	26	QAB(11.5)

PERPENDICULAR SPECTRUM

H (KG)	ΔH(G)	ASSIGNMENT
4.970	-1	RAB(4.5)
7.380	-7	RAB(5.5)
9.366	-9	RAB(6.5)
11.256	-18	RAB(7.5)
13.139	-22	RAB(8.5)
15.049	-21	RAB(9.5)
17.0070	-19	RAB(10.5)
2.5522	-8	RAB(4.5)
1.741	4	RAB(5.5)
1.384	2	RAB(6.5)
1.160	-1	RAB(7.5)
1.008	1	RAB(8.5)
0.893	2	RAB(9.5)
0.805	4	RAB(10.5)
0.730	2	RAB(11.5)
0.663	-3	RAB(12.5)

TABLE 1-S
15(3,12)-14(2,13)
LASER = 127.481 CM-1
PARALLEL SPECTRUM

H (KG)	ΔH(G)	ASSIGNMENT
2.165	7	QBA(-2.5)
2.588	2	QBA(-1.5)
3.128	0	QBA(-0.5)
3.802	1	QBA(0.5)
4.604	1	QBA(1.5)
5.524	-1	QBA(2.5)
6.549	-1	QBA(3.5)
7.664	1	QBA(4.5)
8.846	0	QBA(5.5)
10.096	6	QBA(6.5)
11.393	4	QBA(7.5)
12.745	5	QBA(8.5)
14.148	7	QBA(9.5)
15.604	11	QBA(10.5)
17.117	19	QBA(11.5)

PERPENDICULAR SPECTRUM

H (KG)	ΔH(G)	ASSIGNMENT
6.050	0	RBA(2.5)
7.137	2	RBA(3.5)
8.297	-4	RBA(4.5)
9.535	-2	RBA(5.5)
10.831	-4	RBA(6.5)
12.181	-10	RBA(7.5)
13.595	-7	RBA(8.5)
15.062	-7	RBA(9.5)
16.579	-15	RBA(10.5)

TABLE 1-T
15(3,13)-14(2,12)
LASER = 127.481 CM-1
PARALLEL SPECTRUM

H (KG)	ΔH(G)	ASSIGNMENT
10.096	1	QBA(10.5)
12.4350	9	QBA(11.5)
14.575	19	QBA(12.5)
16.662	15	QBA(13.5)
4.167	0	QBA(10.5)
3.435	-2	QBA(11.5)

PERPENDICULAR SPECTRUM

H (KG)	ΔH(G)	ASSIGNMENT
8.7363	-3	RBA(9.5)
11.4845	-9	RBA(10.5)
13.7830	-11	RBA(11.5)
15.989	-17	RBA(12.5)
4.8968	-1	RBA(9.5)
3.7894	0	RBA(10.5)
3.217	-1	RBA(11.5)

TABLE 1-U
19(3,16)-18(2,17)
LASER = 137.461 CM-1
PARALLEL SPECTRUM

H (KG)	ΔH(G)	ASSIGNMENT
16.225	-43	QAA(-4.5)
14.857	-12	QAA(-3.5)
13.732	-3	QAA(-2.5)
12.803	3	QAA(-1.5)
12.031	16	QAA(-0.5)
11.362	13	QAA(0.5)
10.791	12	QAA(1.5)
10.299	13	QAA(2.5)
9.869	10	QAA(3.5)
9.492	5	QAA(4.5)
9.168	7	QAA(5.5)
8.879	2	QAA(6.5)
8.627	-1	QAA(7.5)
8.409	-5	QAA(8.5)
8.223	-7	QAA(9.5)
8.065	-10	QAA(10.5)
7.938	-11	QAA(11.5)
7.835	-18	QAA(12.5)
7.765	-22	QAA(13.5)
7.734	-23	QAA(14.5)

PERPENDICULAR SPECTRUM

H (KG)	ΔH(G)	ASSIGNMENT
14.901	-22	PAA(-0.5)
13.881	0	PAA(0.5)
13.021	10	PAA(1.5)
12.285	8	PAA(2.5)
11.662	11	PAA(3.5)
11.127	13	PAA(4.5)
10.664	14	PAA(5.5)
10.264	15	PAA(6.5)
9.919	18	PAA(7.5)
9.607	6	PAA(8.5)
9.348	5	PAA(9.5)
13.660	10	RAA(-5.5)
12.649	9	RAA(-4.5)
11.816	14	RAA(-3.5)
11.077	-18	RAA(-2.5)
10.508	14	RAA(-1.5)
9.995	19	RAA(-0.5)
9.538	11	RAA(0.5)
9.139	5	RAA(1.5)
8.793	3	RAA(2.5)
8.488	1	RAA(3.5)
8.220	0	RAA(4.5)
7.982	-3	RAA(5.5)
7.773	-5	RAA(6.5)
7.590	-8	RAA(7.5)
7.431	-11	RAA(8.5)
7.288	-21	RAA(9.5)
7.182	-16	RAA(10.5)

NOTATION

TABLES 1-A TO 1-U, ORDERED BY INCREASING LASER WAVE NUMBER, AND LABELED BY THE ASYMMETRIC ROTOR TRANSITION $N'(K'_a,K'_c) - N''(K''_a,K''_c)$

H = MEASURED MAGNETIC FIELD VALUES IN KILOGAUSS.

$\Delta H = H_{OBS} - H_{CALC}$ FROM LEAST SQUARES FITS, USING EQ. (4) OF THE TEXT. MOLECULAR CONSTANTS OBTAINED ARE GIVEN IN TABLE 3.

ASSIGNMENT - ZEEMAN Q, P, R BRANCHES, LABELED BY M_J OF THE LOWER STATE, AND ORDERED BY POSITIVELY INCREASING M_J VALUES.

Note added in proof. Unfortunately, integral values of ΔH for the computer-printed table 1 were obtained simply by adding 0.5 to the floating point values and truncating. Therefore, all negative entries and some zero entries in the ΔH volumns of Table 1 must be decreased by unity.

Molecular constants obtained directly from the least-squares fits of *individual* Zeeman patterns to Eq. (4) are given in Table 3.

The 79 μm Spectrum (126.437 cm^{-1})

The 79 μm HO_2 laser magnetic resonance spectrum between 0 and 20 kG is shown in Fig. 1 of Ref. (*1*). The low-field transitions near 1 kG have not been assigned. The high-field lines can be grouped into three π branches and four σ branches. Magnetic field values and assignments for lines in these seven Zeeman branches are given in Tables 1-O and 1-P.

As discussed in detail in Ref. (*2*), the analysis of the π and σ branches which form a clear head [Fig. 6 of Ref. (*2*)] leads to a single favored assignment for the running quantum number M_J and for the rotational quantum numbers N' and N''. This part of the 79 μm spectrum corresponds to Eq. (5a) above.

Analysis of the remaining higher-field lines of the 79 μ spectrum also leads to one favored assignment, though somewhat different considerations are required. Since $\Delta E^2 \ll (\delta' - \delta'')^2$, Eqs. (29) and (30) of Ref. (*2*) must be used. Equation (26) of Ref. (*2*) was also helpful. The assignment of the π Zeeman line at 13.7906 kG as Q_{aa} (13.5), with $N'' = 13$, requires a negative sign for δ' and δ''. This higher-field part of the spectrum also corresponds to Eq. (5a) above.

It is felt by the authors that the Zeeman line assignments of the 79 μm spectrum (M_J values) are determined rather unambiguously by the available experimental data.

The asymmetric rotor assignments (*5*) of $14_{3,12}$–$13_{2,11}$ and $14_{3,11}$–$13_{2,12}$ for the two zero-field transitions giving rise to the 79 μ Zeeman spectrum were obtained as follows.

Table 2

Frequencies, Vacuum Wavelengths, and Vacuum Wavenumbers of some H_2O and D_2O CW Laser Lines from Reference (4)[a].

Molecule	Frequency [MHz]	Wavelength [μm]	Wavenumber [cm^{-1}]
H_2O	10 718 068.3	27.970 755	357.516 276
H_2O	3 821 771.3	78.443 328	127.480 567
H_2O	3 790 474.5	79.091 010	126.436 620
H_2O	2 527 952.0	118.591 040	84.323 402
D_2O	4 120 984.3	72.747 780	137.461 240
D_2O	3 557 147.4	84.278 897	118.653 665
D_2O	2 783 066.6	107.720 188	92.833 109

[a] Uncertainties in the above values correspond to ± 1 MHz in the frequency, and arise mainly from irreproducibility in tuning the laser to its maximum power point.

Table 3

Molecular constants obtained from fitting individual Zeeman patterns. The standard deviation σ of each fit is in Gauss. $\Delta H = H_{obs} - H_{calc}$ for each line is in Table 1. The laser mismatch ΔE, spin splitting parameters δ, and spin-free asymmetric rotor transition energies ν_{mol} are shown in Fig. 1 and given here in cm^{-1}; one standard deviation is in parentheses. Asterisks label fits with uncertain M_J numberings.

Table	Laser	$N'(K_a',K_c')$-$N''(K_a'',K_c'')$	σ	ΔE	δ'	δ''	ν_{mol}
1-A	171μ	8(2,7)-8(1,8)	9	-0.235(1)	-0.556(1)	-0.148(0)	58.836
1-B	119μ	4(3,2)-5(2,3)	29	-1.025(9)	-1.993(10)	-0.813(2)	85.200
1-C	119μ	4(3,1)-5(2,4)	27	-1.031(8)	-1.994(10)	-0.813(2)	85.206
1-D	119μ	13(2,12)-12(1,11)	7	+0.784(0)	-0.389(1)	-0.145(0)	83.530
1-E	119μ	11(2,9)-10(1,10)	11	+0.928(1)	-0.444(1)	-0.112(1)	83.381
1-F	119μ	14(2,13)-13(1,12)	11	-0.979(1)	-0.380(2)	-0.136(1)	85.294*
1-G	119μ	12(2,10)-11(1,11)	12	-1.601(2)	-0.405(5)	-0.106(3)	85.912*
1-H	108μ	18(4,15)-19(3,16)	5	+0.162(1)	-1.025(1)	-0.591(0)	92.658
1-I	108μ	18(4,14)-19(3,17)	5	+0.145(0)	-1.024(1)	-0.591(0)	92.675
1-J	108μ	15(2,13)-14(1,14)	10	-0.968(0)	-0.364(1)	-0.086(1)	93.792
1-K	84μ	11(3,8)-10(2,9)	17	-1.293(5)	-0.923(7)	-0.447(2)	119.928
1-L	84μ	11(3,9)-10(2,8)	14	-1.219(3)	-0.920(4)	-0.450(1)	119.854
1-M	84μ	10(3,7)-9(2,8)	11	+0.880(2)	-0.974(2)	-0.500(1)	117.754*
1-N	84μ	10(3,8)-9(2,7)	8	+0.933(1)	-0.979(2)	-0.499(1)	117.701*
1-O	79μ	14(3,12)-13(2,11)	26	+0.228(1)	-0.760(1)	-0.389(0)	126.197
1-P	79μ	14(3,11)-13(2,12)	24	+0.011(0)	-0.735(1)	-0.383(1)	126.415
1-Q	78μ	14(3,12)-13(2,11)	10	+1.262(2)	-0.762(3)	-0.360(1)	126.206
1-R	78μ	14(3,11)-13(2,12)	13	+1.062(1)	-0.756(2)	-0.364(1)	126.406
1-S	78μ	15(3,12)-14(2,13)	8	-1.119(1)	-0.722(2)	-0.342(1)	128.589
1-T	78μ	15(3,13)-14(2,12)	11	-0.851(1)	-0.714(2)	-0.354(1)	128.321
1-U	73μ	19(3,16)-18(2,17)	14	+0.184(0)	-0.601(1)	-0.311(0)	137.270*
	73μ	19(3,16)-18(2,17)	14	+0.160(0)	-0.572(1)	-0.303(0)	137.295*

Values for K_a' and K_a'' were obtained as described in Ref. (*1*) from the theoretical expectation for prolate near-symmetric rotors (*6*)

$$(\delta'/\delta'') \cong (K'^2/K''^2). \tag{6}$$

These K assignments were consistent with energy considerations based on an approximate value for the rotational constant A of 20 cm^{-1} determined from ab initio structure calculations (*7*). Values for N' and N'' were taken directly from the Zeeman assignment. Values of K_c' and K_c'' were obtained by using the *b*-type selection rules (*5*) appropriate for $\Delta K_a = \pm 1$ transitions, the signs and relative magnitudes of $K_a = 2$ and $K_a = 3$ asymmetry splittings (*5*), and the two values of ΔE obtained from the Zeeman assignments (Table 3).

The 119 μm Spectrum (84.323 cm^{-1})

The 119 μm HO_2 magnetic resonance spectrum between 0 and 23 kG is shown in Fig. 2. An enlarged portion of the π spectrum between 7.5 and 10.0 kG is shown in Fig.

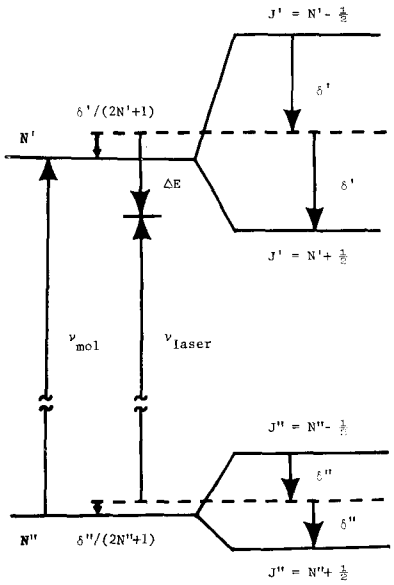

FIG. 1. Schematic illustration of the quantities ν_{mol}, ν_{laser}, ΔE, δ', and δ''. The solid lines represent on the left asymmetric rotor energy levels characterized by a rotational quantum number N, and on the right the spin–split levels arising from a spin–rotation interaction of the form $\mathbf{N}\cdot\mathbf{S}$ for $S = \frac{1}{2}$. The solid lines at the left lie at the centers of gravity of the degeneracy-weighted spin–split levels. The dashed lines represent energy midpoints between the spin–split levels. Upward- and downward-pointing arrows in this diagram (and in corresponding diagrams, if care is taken to use analogous initial and final points for the arrows) indicate positive and negative quantities, respectively, in the notation of this paper.

3 to illustrate the resolution and signal-to-noise ratio obtained. The Zeeman lines in the 119 μm spectrum can be grouped into 6 π and 12 σ branches. Magnetic field values and assignments for the lines in these 18 branches are given in Tables 1-B to 1-G.

Two of the high-field π branches are significantly broader than all the others, with unresolved or barely resolved hyperfine structure. These two branches, together with their associated four σ branches can be assigned quite unequivocally to the $4_{3,1}$–$5_{2,4}$ and $4_{3,2}$–$5_{2,3}$ zero-field asymmetric rotor transitions. The two Zeeman patterns associated with these transitions represent almost perfect cases for application of the arguments used in carrying through the example in Ref. (*2*). They correspond to Eq. (5a). The two Q_{bb} (4.5) Zeeman line assignments require δ' and δ'' to be negative.

The two lowest-field π branches and their associated four σ branches can be fairly unequivocally assigned to the transitions $11_{2,K_c'}$–$10_{1,K_c''}$ and $13_{2,K_c'}$–$12_{1,K_c''}$ on the basis of an analysis as described in Ref. (*2*). Since only one component of each asymmetry doublet is seen in both cases, it is not possible from the Zeeman spectrum alone to choose between the two possible sets of K_c values. The assignments $11_{2,9}$–$10_{1,10}$ and $13_{2,12}$–$12_{1,11}$ were chosen later to bring the observed zero-field energy levels obtained from ($\nu_{laser} - \Delta E$) into agreement with the asymmetric rotor fits. The lines $Q_{ab}(-12.5)$ in Table 1-D and $Q_{ab}(-10.5)$ in Table 1-E require δ' and δ'' to be negative. The Zeeman patterns for both transitions correspond to Eq. (5c) above.

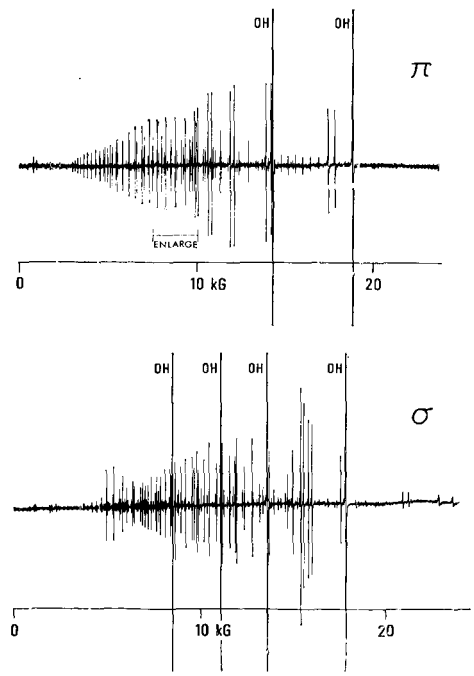

FIG. 2. The 119 μm laser magnetic resonance spectrum of HO_2 in parallel (π) and perpendicular (σ) polarization. Source oscillator: H_2O laser. HO_2 is produced by reacting a mixture of oxygen atoms and oxygen molecules with ethylene at a total pressure of 1.1 Torr. Zeeman modulation at 100 Hz is used with a detector time constant of 0.1 sec.

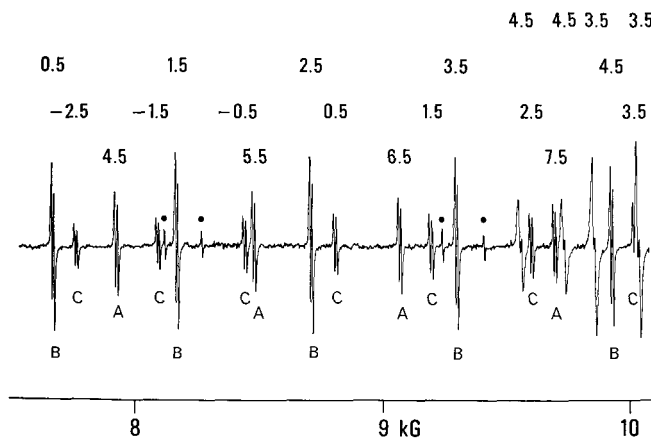

FIG. 3. An enlarged display of the 7.5–10.0 kG region of the π spectrum shown in Fig. 2. Three branches with completely resolved hyperfine structure can clearly be seen, as well as the first two lines of two branches with only barely resolved hyperfine structure. The M_J values above each Zeeman line correspond to those given in Tables 1-B to 1-G. (The arbitrary branch labels *A*, *B*, *C* in the figure correspond to Tables 1-D, 1-E, 1-F, respectively.) The full circles over weak features indicate O_2 impurity lines.

Analysis as described in Ref. (*2*) leads to a large number of acceptable M_J assignments for the remaining two π branches and associated four σ branches of the 119 μm spectrum. M_J numberings and the asymmetric rotor assignments $14_{2,13}$–$13_{1,12}$ and $12_{2,10}$–$11_{1,11}$ were finally chosen to bring the zero-field energy levels obtained from a fit using Eq. (4) into agreement with asymmetric rotor calculations. Because of the uncertain M_J numberings, these six Zeeman branches could not be used to give independent support to the zero-field assignments and molecular constants obtained in this paper. The analyses of these branches presented here are merely consistent with those assignments and constants. The Zeeman patterns for these two transitions correspond to Eq. (5c).

The 84 μm Spectrum (118.654 cm^{-1})

The π and σ spectra obtained using this D_2O laser line as a fixed-frequency radiation source are illustrated in Fig. 3 of Ref. (*1*). Magnetic field values and assignments of the Zeeman transitions in the 84 μm spectrum are given in Tables 1-K to 1-N.

Two high-field π branches in the 84 μm spectrum can be chosen (with some difficulty) which lead to an unambiguous M_J assignment from Eq. (1) above. This assignment requires a negative value of c and corresponds to Eq. (5b), so that Zeeman lines characterized by exactly the same upper- and lower-state quantum numbers can occur at two different magnetic fields (*2*). Two high-field σ branches can also be picked out. These four branches are sufficient to allow trial fits to Eqs. (1) and (2) above. Equations (25) and (40) of Ref. (*2*) were used to extend the branches to weaker lines. The final fit of these Zeeman patterns is characterized by very secure M_J numberings, but by an uncertainty of several units in the N' and N'' values. The assignments $11_{3,8}$–$10_{2,9}$ and $11_{3,9}$–$10_{2,8}$ were chosen to bring the calculated zero-field rotational energy levels into crude agreement with the symmetric top expression (*5*)

$$E_{\text{rot}} \approx \bar{B}N(N+1) + (A - \bar{B})K^2, \tag{7}$$

with the two constants A and $\bar{B}$ determined from Eq. (7) and the $4_{3,K_c'}$–$5_{2,K_c''}$ and $14_{3,K_c'}$–$13_{2,K_c''}$ transitions described earlier.

After all Zeeman lines belonging to the $11_{3,K_c'}$–$10_{2,K_c''}$ patterns had been assigned, four strong π and four strong σ lines remained unassigned. Once molecular constants were firmly established by asymmetric rotor fits of securely assigned rotational transitions, these eight lines could be assigned to Zeeman components of $10_{3,7}$–$9_{2,8}$ and $10_{3,8}$–$9_{2,7}$, as indicated in Tables 1-M and 1-N. These patterns also correspond to Eq. (5b). Their assignments do not represent independent support for the results of this paper; they are merely consistent with those results.

The 78 μm Spectrum (127.481 cm^{-1})

The spectrum obtained with this H_2O laser line is not shown, but it can be divided quite easily into four π branches and four σ branches. Magnetic field values and assignments for these branches are given in Tables 1-Q to 1-T.

Two sets of π, σ branches can be subjected to the treatment outlined in Ref. (*2*) to obtain unambiguous M_J numberings and unambiguous values for the quantum numbers N' and N''. As it happens, fits to these two sets of Zeeman branches yield the zero-

field $14_{3,12}$–$13_{2,11}$ and $14_{3,11}$–$13_{2,12}$ asymmetric rotor frequencies already obtained from the 79 μm spectrum, though the 78 μm Zeeman patterns here correspond to Eqs. (5c) and (5b) above, respectively, rather than to Eq. (5a) as the 79 μm spectra do. The $Q_{ab}(-13.5)$ line in Table 1-Q requires δ' and δ'' to be negative.

It is interesting to note that the zero-field 14–13 rotational transition frequencies ν_{mol} determined from the 78 μm and 79 μm laser magnetic resonance spectra agree to 0.009 cm^{-1}, but that the corresponding spin splittings 2δ agree to only 0.06 cm^{-1}. These discrepancies indicate the size of errors associated with the (derived) zero-field energy differences. It would appear a priori that magnetic field uncertainties of 1 G should correspond to energy uncertainties of approximately 0.000 05 cm^{-1}. Unfortunately, however, model errors associated with least-squares fits of the Zeeman branches using Eq. (4) are quite large, i.e. at least 0.009 cm^{-1} in the determination of asymmetric rotor transition frequencies and at least 0.06 cm^{-1} in the determination of spin splittings.

The remaining lines in the 78 μm spectrum can be assigned to Zeeman components of $15_{3,12}$–$14_{2,13}$ and $15_{3,13}$–$14_{2,12}$, corresponding to Eqs. (5c) and (5b), respectively. The M_J assignments can be made unambiguously using the treatment of Ref. (*2*), but the N assignments must be chosen to bring the resultant zero-field rotational transitions into agreement with those expected from Eq. (7), the ab initio structure (*7*), and the $14_{3,K_c'}$–$13_{2,K_c''}$ results determined above.

The 108 μm Spectrum (92.833 cm^{-1})

The magnetic resonance spectrum obtained with this D_2O laser line (not shown) is extremely rich and not very pretty, with many overlapped lines and branches. In contrast to the spectra obtained with the four preceding laser lines, only a small portion of the 108 μm spectrum is assigned. Magnetic field values and assignments for this small portion are given in Tables 1-H to 1-J.

Two high-field π branches and two high-field σ branches with only partially resolved hyperfine splittings can be picked out of the spectrum by inspection. Strict application of the methods of Ref. (*2*) lead to ambiguity both in the M_J numberings and in the N assignments for these branches. The N'–N'' assignment of the zero-field transitions can be established as 18–19 from expectations based on Eq. (7), once the K_a assignment has been settled from considerations based on Eq. (6). From this N'–N'' assignment, from trial fits to Eqs. (1) and (2), and from careful intensity and line shape considerations (*2*), a convincing argument in favor of one particular M_J assignment of the π and σ branches can be made. The final assignments of the lines to Zeeman components of the transitions $18_{4,15}$–$19_{3,16}$ and $18_{4,14}$–$19_{3,17}$, as given in Tables 1-H and 1-I, are believed to be established with reasonable certainty. The Zeeman patterns correspond to Eq. (5a).

One strong low-field π and σ branch with completely resolved hyperfine splitting can also be picked out of the 108 μm spectrum by inspection. Careful application of the treatment of Ref. (*2*), including intensity calculations for the ZR branch, leads to an unambiguous assignment of the spectrum to Zeeman transitions in $15_{2,13}$–$14_{1,14}$, as given in Table 1-J.

The 171 μm Spectrum (58.625 cm^{-1})

The wavenumber of the CH_3OH laser line at 170.5764 μm is 58.625 cm^{-1} (*8*). Many of the observed Zeeman lines in this complicated but well-resolved spectrum are ex-

pected to belong to low N zero-field ${}^{R}Q_1(N)$ transitions. Unfortunately, branches associated with these low N values are very short, and thus difficult to pick out. However, one branch at low field gives a shift $(\Delta H/\Delta\nu)$ in a positive direction when the laser frequency is pulled by detuning the cavity slightly, opposite to most of the remainder of the 171 μm spectrum. It is only this one π branch and its corresponding σ branch which have been assigned. Magnetic field values and assignments for these two branches are given in Table 1-A. The M_J numbering and asymmetric rotor assignment of $8_{2,7}$–$8_{1,8}$ were obtained quite unambiguously using the techniques of Ref. (*2*).

The 73 μm Spectrum (137.461 cm^{-1})

The wavenumber of a cw D_2O laser line at 71.944 μm is 138.99 cm^{-1} (*9*). Since this was the only cw D_2O laser line reported in this region at the beginning of the HO_2 work, the spectrum illustrated in Fig. 2 of Ref. (*1*) is referred to as the 72 μm spectrum. After considerable difficulty in obtaining a zero-field rotational energy difference (i.e., ν_{mol}) from this spectrum consistent with the results from all other spectra mentioned above, it was observed that most of the difficulties could be eliminated by postulating that the D_2O laser used to record the observed spectrum was actually running cw on a neighboring line. Indeed, subsequent measurement (*4*) found a cw line at 72.7478 μm with a wavenumber of 137.461 cm^{-1}. From discussion with several of the authors of (*4*) and (*9*), it seems likely that D_2O can lase cw on either the 71.944 μm or the 72.748 μm line, albeit weakly and unpredictably.

Analysis of the 73 μm spectrum carried out using the techniques of Ref. (*2*) leads to some ambiguity in the M_J numbering and in the N'–N'' assignment of the transition, principally because the π and σ head regions have not been recorded with the same high resolution and signal-to-noise ratio as that shown for the 79 μm spectrum in Fig. 6 of Ref. (*2*). It is possible, however, to choose an M_J numbering and an N'–N'' assignment (and a D_2O laser frequency) which bring the results from this spectrum into good agreement with those obtained from the other spectra above. Magnetic field values and assignments for the observed lines are given in Table 1-U. Unfortunately, an increase in the M_J numbering of all lines by one unit gives results almost equally consistent, as found in the last line of Table 3.

The 392 μm and 496 μm Spectra

Laser magnetic resonance spectra of HO_2 have been found using the 392 μm line of CH_3OH and the 496 μm line of CH_3F. These spectra have not been analyzed.

IV. THE ASYMMETRIC ROTOR FIT

From Eq. (16) of (*2*) and Fig. 1 above we see that a hypothetical asymmetric rotor transition frequency ν_{mol}, free from the effects of electron spin splittings, can be determined for each assigned Zeeman pattern from the expression

$$\nu_{\text{mol}} = \nu_{\text{laser}} - \Delta E + [\delta'/(2N' + 1) - \delta''/(2N'' + 1)]. \tag{8}$$

The quantity ν_{mol} is given in Table 3 for each zero-field transition assigned.

Table 4

Asymmetric rotor fit of the zero-field spin-free rotational transitions ν_{mol} found in Table 3 from analyses of the spectra in Table 1. Asterisks indicate transitions not used in the fit. The standard deviation of the fit is 0.008 cm^{-1}; the six rotational constants obtained are in Table 5.

$N'(K'_a,K'_c)$-$N''(K''_a,K''_c)$	ν_{mol} [cm^{-1}]	$\nu_{obs}-\nu_{calc}$
8(2,7)-8(1,8)	58.836	+0.007
4(3,2)-5(2,3)	85.200	-0.003
4(3,1)-5(2,4)	85.206	-0.002
13(2,12)-12(1,11)	83.530	-0.002
11(2,9)-10(1,10)	83.381	-0.007
14(2,13)-13(1,12)	85.294*	+0.002
12(2,10)-11(1,11)	85.912*	-0.014
18(4,15)-19(3,16)	92.658	-0.001
18(4,14)-19(3,17)	92.675	-0.000
15(2,13)-14(1,14)	93.792	-0.001
11(3,8)-10(2,9)	119.928	+0.008
11(3,9)-10(2,8)	119.854	+0.007
10(3,7)-9(2,8)	117.754*	-0.003
10(3,8)-9(2,7)	117.701*	-0.007
14(3,12)-13(2,11)	126.197	-0.015
14(3,11)-13(2,12)	126.415	+0.002
14(3,12)-13(2,11)	126.206	-0.006
14(3,11)-13(2,12)	126.406	-0.007
15(3,12)-14(2,13)	128.589	+0.008
15(3,13)-14(2,12)	128.321	+0.010
19(3,16)-18(2,17)	137.270*	-0.010
19(3,16)-18(2,17)	137.295*	+0.015

The error to be associated with ν_{mol} is approximately the same as that associated with ΔE, since the values for ν_{laser} have been very precisely measured (*4*, *8*), and since the errors in δ' and δ'' must be divided by $2N$ in Eq. (8). One standard deviation for the parameters ΔE, δ', δ'' from the least-squares fits of the Zeeman patterns is given in parentheses following the corresponding quantities in Table 3, and indicates uncertainties in the last digit. These uncertainties are unrealistically small, however, since large model errors remain in the Zeeman pattern fits. This conclusion can be deduced most convincingly from the size and systematic nature of the observed–minus–calculated magnetic field values (ΔH) given in Tables 1-A to 1-U. A more reliable estimate of the errors in ν_{mol} can be obtained by comparing the values obtained from the 78 μm spectrum and from the 79 μm spectrum for each of the transitions $14_{3,12}$–$13_{2,11}$ and $14_{3,11}$–$13_{2,12}$: the disagreement is seen to be 0.009 cm^{-1} in one case and 0.009 cm^{-1} in the opposite sense in the other. It thus seems likely that ν_{mol} values are determined in this work to no better than ± 0.01 cm^{-1}.

Table 5

Rotational constants A,B,C and symmetric-top centrifugal distortion constants D_K, D_{NK}, D_N in cm^{-1} for HO_2, obtained from an asymmetric rotor fit to 14 transitions in Table 4, and compared to A,B,C from ab initio calculations.

	This work[a,b]	SCF[c]	CI[c]
A	20.358(3)	21.368	20.577
B	1.1179(5)	1.035	0.938
C	1.0567(5)	0.987	0.897
D_K	0.0041(3)		
D_{NK}	0.00012(1)		
D_N	0.0000042(8)		

[a] Standard deviation of the fit σ = 0.008 cm^{-1}, one standard deviation of each parameter is given in parentheses.

[b] Inertial defect Δ = +0.045 $uÅ^2$.

[c] Self-consistent-field and configuration-interaction results from (7).

A second kind of uncertainty enters into the values of ν_{mol}. As mentioned in Section III above, the treatment outlined in Ref. (*2*) did not, in some cases, yield unambiguous M_J assignments for the lines in the Zeeman patterns. The values of ν_{mol} indicated by asterisks in Table 3 correspond to patterns where the M_J numbering is in doubt. Since a shift in the M_J numbering by one unit can cause a change in the value of ΔE of 0.02–0.04 cm^{-1}, these values of ν_{mol} were not used in the asymmetric rotor fit.

Table 4 gives the results of a least-squares fit of the zero-field asymmetric rotor transitions using a program written by Maki (*10*) based on Watson's centrifugal distortion Hamiltonian (*11–13*). Since the three rotational constants (A, B, C) and the three symmetric-top centrifugal distortion constants (D_K, D_{NK}, D_N) were sufficient to give a good fit to the data, the results in Table 4 correspond to a fit using the relatively simple rotational Hamiltonian

$$H_r = AN_z^2 + BN_x^2 + CN_y^2 - D_K N_z^4 - D_{NK} N^2 N_z^2 - D_N N^4, \tag{9}$$

where $\mathbf{N} \equiv \mathbf{J} - \mathbf{S}$ represents the rotational angular momentum operator. The inclusion of the two asymmetric-top centrifugal distortion constants δ_K and δ_N did not improve the fit significantly.

Table 5 gives the three rotational constants and three centrifugal distortion constants obtained from the fit of Table 4. One standard deviation is given in parentheses after each constant, and represents the uncertainty in the last digit. The small positive inertial defect is consistent with that expected for a planar molecule (*14*). The constants $\mathfrak{A}$, $\mathfrak{B}$, $\mathfrak{C}$, Δ_K, Δ_{NK}, Δ_N from a fit using all *five* centrifugal distortion parameters agree with the corresponding constants in Table 5 to within their respective standard deviations.

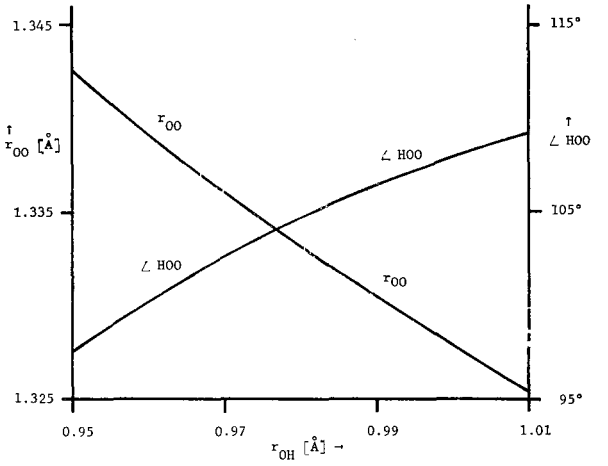

FIG. 4. Values for the O–O bond length in Å (left abscissa) and the HOO angle in degrees (right abscissa), calculated from the rotational constants A and B of Table 5 as a function of various assumed values of the O–H bond length.

The experimentally obtained rotational constants can be compared with those obtained from a structure given by ab initio self-consistent-field (SCF) or configuration–interaction (CI) calculations (*7*). It can be seen from Table 5 that the quantitative agreement is good. It can also be seen, however, that the values for B and C, which are quite sensitive to the O–O distance, are worse for the more complete CI calculation. This result was anticipated by the authors of Ref. (*7*), who wrote, "Nevertheless, in light of the known inadequacy of our basis set, it seems likely that the O–O distance in HO_2 is more accurately predicted by our SCF calculation than our energetically superior CI treatment."

It is, of course, not possible to determine the full geometry of a bent triatomic XYZ molecule from the three rotational constants of a single isotope. However, by assuming one of the three structural parameters, the other two can be calculated. Figure 4 gives a plot of both the O–O bond length and the HOO angle calculated from the rotational constants A and B of Table 5 for various assumed values of the O–H bond length.

V. THE SPIN-SPLITTING FIT

The spin-splitting parameter δ for each asymmetric rotor rotational level $N_{K_aK_c}$ is defined by the expression

$$2\delta = F_1(K_a, K_c, N, J = N + \tfrac{1}{2}) - F_2(K_a, K_c, N, J = N - \tfrac{1}{2}), \qquad (10)$$

where F_1 and F_2 represent standard diatomic notation (*15*) for the two spin components of given N in a doublet state. The parameters δ, which are obtained directly from the fits to the Zeeman patterns described in Section III, are given in Table 3 for the zero-field transitions assigned in this work. One standard deviation from the fit is given in parentheses following the value of δ, and represents the uncertainty in the last digit. Just as for ΔE, this uncertainty is unrealistically small. Comparison of δ values determined for the same rotational energy level $N_{K_aK_c}$ from two or three different laser Zeeman patterns

Table 6

A fit of observed spin splitting parameters δ in cm^{-1} to Eq. (11). The standard deviation σ of the fit is 0.012 cm^{-1}. Constants obtained from the fit are given in Eqs. (12). Asterisks indicate values of δ not used in the fit.

N	K_a	K_c	δ	$\delta_{obs} - \delta_{calc}$	N	K_a	K_c	δ	$\delta_{obs} - \delta_{calc}$
8	1	8	-0.148	-0.004	12	2	a	-0.405*	-0.001
10	1	10	-0.112	+0.009	13	2	a	-0.377	+0.004
11	1	11	-0.106*	+0.007	14	2	a	-0.348	+0.014
12	1	11	-0.145	+0.018	15	2	a	-0.364	-0.018
13	1	12	-0.136*	+0.026	18	2	a	-0.311*	-0.001
14	1	14	-0.086	+0.011	4	3	a	-1.993	+0.010
5	2	a	-0.813	+0.002	10	3	a	-0.976*	+0.008
8	2	a	-0.556	-0.002	11	3	a	-0.921	-0.013
9	2	a	-0.499*	+0.005	14	3	a	-0.753	-0.009
10	2	a	-0.448	+0.016	15	3	a	-0.718	-0.014
11	2	a	-0.444	-0.013	19	3	a	-0.591	-0.004
					18	4	a	-1.024	+0.005

[a] Entries for δ in this table for $K_a \neq 1$ are averages (when possible) of values having the same N and K_a, but different K_c.

yields discrepancies ranging from 0.002 to 0.038 cm^{-1}. Uncertainties in the δ values determined in this work are thus probably of the order of ± 0.03 cm^{-1}.

The quantity δ can be related to a spin–rotation interaction tensor ϵ, whose components are expected to vary slowly with changes in the rotational quantum numbers (*6*). Allowing for $\Delta K = 0$, $\Delta N = \pm 1$ interactions, but not for $\Delta K \neq 0$ interactions, a slight extension of the expression in Ref. (*6*) is obtained.

$$\delta = \tfrac{1}{2}(N+\tfrac{1}{2})\{+\tfrac{1}{2}(\epsilon_{bb}+\epsilon_{cc}) - \tfrac{1}{4}(\epsilon_{bb}-\epsilon_{cc})\delta_{K_a,1}(-1)^{N-K_c} + \epsilon_{ll}[K_a^2/N(N+1)] - [\epsilon_{ll}^2/2(B+C)][K_a^2/N(N+1)][1 - K_a^2(N^2+N+1)/N^2(N+1)^2]\}. \quad (11)$$

Since Eq. (11) involves only the rotational constants N and K_a for $K_a \neq 1$, the parameters δ in Table 3 for given N and $K_a \neq 1$ but different K_c were averaged before carrying out the least-squares fit to Eq. (11) presented in Table 6. Values of the constants obtained from this fit are given in Eqs. (12), with one standard deviation in parentheses.

$$\begin{aligned} \epsilon_{ll} \equiv \epsilon_{aa} - \tfrac{1}{2}(\epsilon_{bb}+\epsilon_{cc}) &= -1.637(8)\ cm^{-1}, \\ \tfrac{1}{2}(\epsilon_{bb}+\epsilon_{cc}) &= -0.0072(6)\ cm^{-1}, \\ \tfrac{1}{2}(\epsilon_{bb}-\epsilon_{cc}) &= -0.009(2)\ cm^{-1}. \end{aligned} \quad (12)$$

Equation (11) should actually involve the two additional parameters ϵ_{ab} and ϵ_{ba}. They are absent because $\Delta K = \pm 1$ matrix elements have been neglected.

Note that the sign of the dominant spin-splitting constant ϵ_{aa} is negative here, the same as that found for ClO_2 (*16*), but opposite to that found for NO_2 (*17*). (The sign of ϵ_{aa} for HO_2 was incorrectly assumed to be positive in (*1*).) While a quantitative treatment similar to that for ClO_2 (*18*) has not been carried out, it seems likely, by analogy

with atomic spectroscopy (*19*), that the negative sign of ϵ_{aa} is associated with the fact that HO_2 and ClO_2 contain a π^3 open shell (one hole) in the linear configuration, while NO_2 contains a π^1 open shell (one electron).

VI. POSSIBLE SPECTRUM OF AN EXCITED STATE

A new spectrum arises in the 84 μm Zeeman pattern when the conditions of HO_2 generation described in Ref. (*1*) are altered. This new spectrum, which is barely visible under the experimental conditions described in Ref. (*1*), can in fact be made stronger than the "normal" 84 μm spectrum shown in Fig. 3 of (*1*).

Using the oxygen–ethylene source, the new lines are enhanced by adding large amounts of O_2 through the microwave discharge. The most probable stable product of discharging excess O_2 is the electronic metastable molecule O_2 ($a^1\Delta_g$). Although the necessary systematic experiments to determine the origin of the new spectrum have not yet been performed, it seems possible that we have observed HO_2 in the excited electronic state $^2A'$. This is supported by the recent report of infrared emission from HO_2 ($^2A' \rightarrow {}^2A''$) by Becker *et al.* (*20*) under very similar chemical conditions, and by the report of an infrared absorption spectrum of HO_2 ($^2A' \leftarrow {}^2A''$) by Hunziker and Wendt (*21*). These observations agree very well with the predicted location of the $^2A'$ state by Gole and Hayes (*22*) from nonempirical LCAO MO SCF and CI calculations.

Becker *et al.* (*20*) suggest that the HO_2 ($^2A'$) state is populated by energy transfer from O_2 ($a^1\Delta_g$)

$$HO_2\ (^2A'') + O_2\ (a^1\Delta_g) \rightarrow HO_2\ (^2A') + O_2(^3\Sigma_g^-), \tag{13}$$

either directly or through subsequent collision-induced intramolecular energy transfer.

No attempts have been made to observe related new spectra with other laser lines.

VII. DISCUSSION

In the present work we have made firm M_J assignments in 16 Zeeman patterns occurring in magnetic resonance spectra obtained with six different cw laser lines. Tentative M_J assignments are proposed for five other patterns.

These M_J assignments lead to a set of zero-field molecular energy levels which conform closely to those expected for a near-prolate asymmetric rotor in a doublet electronic spin state, with the principal spin-splitting contribution arising from the interaction of electron spin and molecular rotation. The magnitudes of the rotational constants A, B, C obtained from the asymmetric rotor energy levels point strongly to a bent triatomic molecule containing two first-row atoms plus hydrogen. Even though isotopic spectra have not been analyzed, the above spectroscopic results, together with the chemical and hyperfine-splitting evidence cited in Ref. (*1*), make it virtually certain that the observed magnetic resonance spectra arise from the free radical HO_2.

There are several possible courses for future work. The isotopic species DO_2 could be investigated in a fashion identical to that described in Refs. (*1, 2*) and here for HO_2, in order to fix the molecular geometry. This is of particular interest since the rather low OH-stretching frequency of 3414 cm^{-1} found in matrix isolation studies (*23, 24*) suggests an OH bond significantly longer than that found in H_2O.

It should also be possible to refine the theory used in carrying out the final least-squares fits of the Zeeman patterns obtained (using the now known rotational constants

Table 7

Calculated $\Delta K_a = 0$, $\Delta J = \Delta N$ Transition Frequencies for $N = 1 \leftarrow 0$ and $2 \leftarrow 1$ Transitions in HO_2

Transition	Frequency [GHz]	
$1_{01} - 0_{00}$	65.2 ± 1.5	
$2_{12} - 1_{11}$	117.7 ± 1.5	($J = N-\frac{1}{2}$)
$2_{11} - 1_{10}$	121.5 ± 1.5	($J = N-\frac{3}{2}$)
$2_{02} - 1_{01}$	130.4 ± 1.5	
$2_{12} - 1_{11}$	131.3 ± 1.5	($J = N+\frac{1}{2}$)
$2_{11} - 1_{10}$	134.8 ± 1.5	($J = N+\frac{3}{2}$)

to take into account $\Delta N = \pm 1$ matrix elements, for example), so that the molecular constants obtained from such fits would reflect only the small experimental uncertainties in magnetic field measurement, and not the large model errors present in this work.

A second experimental course would be to use the energy levels and chemical preparation schemes now known to help in carrying out conventional microwave searches for transitions in HO_2. Such *zero-field* experimental data would, of course, obviate the additional theoretical work mentioned in the previous paragraph.

There is undoubtedly significant information in the numerous proton hyperfine splittings clearly observable in the spectrum. These hyperfine splittings have not been considered theoretically at all.

It is, of course, of interest to look for radiofrequency signals from HO_2 in the interstellar medium. At the present time, the large uncertainties in the calculated asymmetric rotor energy levels and in the calculated spin splittings lead to quite large search ranges. Nevertheless, it is perhaps of interest to note that the present work leads to the predicted *a*-type ($\Delta K_a = 0$) $N = 1 \leftarrow 0$ and $2 \leftarrow 1$ transitions given in Table 7. Unfortunately, no experimental information is available concerning $K_a = 0$ spin splittings, though they are expected theoretically to be considerably smaller than the $K_a = 1$ splittings for the same N values. Thus, the $K_a = 0$ transition frequencies in Table 7 represent pure asymmetric rotor frequencies, corresponding to vanishingly small spin splittings (or spin *shifts* when $N = 0$). The error limits in Table 7 were obtained essentially by increasing the 0.03 cm^{-1} uncertainties in spin-splitting determinations (Section V) by 50%. It should further be noted that no $\Delta K_a = 0$ transitions were seen in the present work, since they fall at much too low frequencies.

ACKNOWLEDGMENTS

The authors are indebted to Dr. W. J. Lafferty for extensive suggestions and discussions of recent spin–rotational results in the infrared spectrum of NO_2, to Professors P. A. Giguère and J. F. Ogilvie for comments concerning OH bond lengths, and to Dr. F. J. Lovas for helpful criticism of the manuscript.

RECEIVED: November 25, 1974

REFERENCES

1. H. E. RADFORD, K. M. EVENSON, AND C. J. HOWARD, *J. Chem. Phys.* **60**, 3178 (1974).
2. J. T. HOUGEN, *J. Mol. Spectrosc.*, in press.

3. J. S. WELLS AND K. M. EVENSON, *Rev. Sci. Instr.* **41**, 226 (1970).
4. F. R. PETERSEN, K. M. EVENSON, AND D. A. JENNINGS, to be published.
5. C. H. TOWNES AND A. L. SCHAWLOW, "Microwave Spectroscopy," McGraw–Hill, New York, 1955.
6. C. C. LIN, *Phys. Rev.* **116**, 903 (1959).
7. D. H. LISKOW, H. F. SCHAEFER III, AND C. F. BENDER, *J. Am. Chem. Soc.* **93**, 6734 (1971).
8. H. R. FETTERMAN, B. J. CLIFTON, P. E. TANNENWALD, AND C. D. PARKER, *Appl. Phys. Lett.* **24**, 70 (1974).
9. W. S. BENEDICT, M. A. POLLACK, AND W. J. TOMLINSON III, *IEEE J. Quant. Elec.* **QE-5**, 108 (1969).
10. A. G. MAKI, private communication.
11. J. K. G. WATSON, *J. Chem. Phys.* **45**, 1360 (1966).
12. J. K. G. WATSON, *J. Chem. Phys.* **46**, 1935 (1967).
13. J. K. G. WATSON, *J. Chem. Phys.* **48**, 4517 (1968).
14. D. R. HERSCHBACH AND V. W. LAURIE, *J. Chem. Phys.* **40**, 3142 (1964).
15. G. HERZBERG, "Spectra of Diatomic Molecules," Van Nostrand, New York, 1950.
16. R. F. CURL, JR., R. F. HEIDELBERG, AND J. L. KINSEY, *Phys. Rev.* **125**, 1993 (1962).
17. G. R. BIRD, J. C. BAIRD, A. W. JACHE, J. A. HODGESON, R. F. CURL, JR., A. C. KUNKLE, J. W. BRANSFORD, J. RASTRUP-ANDERSEN, AND J. ROSENTHAL, *J. Chem. Phys.* **40**, 3378 (1964).
18. R. F. CURL, JR., *J. Chem. Phys.* **37**, 779 (1962).
19. E. U. CONDON AND G. H. SHORTLEY, "Theory of Atomic Spectra," Cambridge, England, 1957.
20. K. H. BECKER, E. H. FINK, P. LANGEN, AND U. SCHURATH, *J. Chem. Phys.* **60**, 4623 (1974).
21. H. E. HUNZIKER AND H. R. WENDT, *J. Chem. Phys.* **60**, 4622 (1974).
22. J. L. GOLE AND E. F. HAYES, *J. Chem. Phys.* **57**, 360 (1972).
23. D. E. MILLIGAN AND M. E. JACOX, *J. Chem. Phys.* **38**, 2627 (1963).
24. M. E. JACOX AND D. E. MILLIGAN, *J. Mol. Spectrosc.* **42**, 495 (1972).